# Electron emission perpendicular to the polarization direction in laser-assisted XUV atomic ionization

A. A. Gramajo and R. Della Picca

*Centro Atómico Bariloche (CNEA) and CONICET, 8400 Bariloche, Argentina*

D. G. Arbó

*Institute for Astronomy and Space Physics IAFE (UBA-Conicet), Buenos Aires, Argentina*

We present a theoretical study of ionization of the hydrogen atom due to an XUV pulse in the presence of an infrared (IR) laser with both fields linearly polarized in the same direction. In particular, we study the energy distribution of photoelectrons emitted perpendicularly to the polarization direction. As we previously showed in Gramajo *et al.* [Phys. Rev. A **94**, 053404 (2016)] for parallel emission, by means of a very simple semiclassical model which considers electron trajectories born at different ionization times, the electron energy spectrum can be interpreted as the interplay of *intra-* and *intercycle* interferences. However, contrary to the case of parallel emission the intracycle interference pattern stems from the coherent superposition of four electron trajectories giving rise to (i) interference of electron trajectories born during the same half cycle (intra-half-cycle interference) and (ii) interference between electron trajectories born during the first half cycle with those born during the second half cycle (inter-half-cycle interference). The intercycle interference is responsible for the formation of the sidebands. We also show that the destructive inter-half-cycle interference for the absorption and emission of an even number of IR laser photons is responsible for the characteristic sidebands in the perpendicular direction separated by twice the IR photon energy. This contrasts with the emission along the polarization axis (all sideband orders are present) since intra-half-cycle interferences do not exist in that case. The intracycle interference pattern works as a modulation of the sidebands and, in the same way, it is modulated by the intra-half-cycle interference pattern. We analyze the dependence of the energy spectrum on the laser intensity and the time delay between the XUV pulse and the IR laser. Finally, we show that our semiclassical simulations are in very good agreement with quantum calculations within the strong-field approximation and the numerical solution of the time-dependent Schrödinger equation, giving rise to nonzero emission, in contraposition to other theories.

## I. INTRODUCTION

More than twenty years have passed since the publication of one of the first theoretical predictions of sidebands in laser assisted photoelectric effect (LAPE) [1]. The simultaneous absorption of one high-frequency photon and the exchange of several additional photons from the laser field lead to equally spaced sideband peaks in the photoelectron (PE) spectra. Since this pioneer work, a lot of experiments have been performed in this area. Typically, the XUV + IR (infrared) field was first obtained through high-order harmonic generation using the original IR laser field as its source [2–5]. In contrast to this kind of XUV radiation generation, the monochromaticity of the femtosecond XUV pulse from a free electron laser (FEL) enables the study of two-color multiphoton ionization without additional overlapping contributions from neighboring harmonics [6–11].

Several studies have been performed to analyze the PE emission in LAPE depending on different features of the fields: Temporal duration, intensity, polarization state, etc. For example, the temporal overlap between the XUV and IR pulses establishes two well distinguished regimes according to whether the XUV pulse duration is greater or less than the laser optical period [8,12,13]. Whereas in the former, the laser intensity is directly related, in a nontrivial way, to the intensity of the appearing sideband peaks in the PE spectrum [8,14,15], the latter has been used to characterize the shape and duration

of an IR laser pulse with a technique called "streak camera" [16–19]. Furthermore, the variation of the polarization states of each field gives rise to dichroic effects in the PE spectrum, which opens the door to the control of the electronic emission [6,9,20–24].

Hitherto, most of the PE spectra have been measured with angle integrated resolution. Only very recently has it been possible to measure angularly resolved PE spectra [11,15,23–26], which is fundamental to achieving a complete understanding of the LAPE process. In contrast to experiments, theoretical analysis restricted to fixed emission angles does not present major difficulties. Most of the theories of LAPE processes are based on the strong-field approximation (SFA) [27–29]. For example, the soft-photon approximation (SPA) [14], derived from the SFA in the velocity gauge for infinitely long XUV and IR pulses, depicts satisfactorily the experimental results [4,6,7,10,11,30]. Besides, the analytic angle-resolved PE spectra derived by Kazansky *et al.* [31,32] and Bivona *et al.* [33] are based on simplifications of the temporal integration within the SFA. Furthermore, in our previous work [34], we have presented a semiclassical approach that describes the XUV + IR multiphoton ionization along the direction of polarization of both fields in very good agreement with the results by solving *ab initio* the time-dependent Schrödinger equation (TDSE). In that work, we have interpreted the PE spectrum as the coherent superposition of electron trajectories

emitted within the same optical cycle leading to an intracycle interference pattern that modulates the sidebands, which can be thought of as a consequence of the intercycle interference of electron trajectories born at different optical cycles.

To the best of our knowledge, LAPE ionization has not been studied in detail for emission directions different from the polarization axis. Furthermore, Haber *et al.* have noted the need for a more comprehensive theoretical description due to the poor agreement between theoretical and experimental PE angular distributions for the two-color two-photon above threshold ionization [25,35]. Several theories, like SPA, predict no emission in the direction perpendicular to the polarization axis. However, Bivona *et al.* envisaged nonzero emission for XUV ionization of hydrogen by short intense pulses [33]. Therefore, in the present paper, we extend our previous work [34] for LAPE from $H(1s)$ to study the emission in the direction perpendicular to the polarization axis of both XUV and laser fields. In contrast to the case of forward emission, we find that transversal emission has relatively low probabilities, i.e., the PE energy range is highly reduced, However, we observe that the PE emission is nonvanishing in agreement with Bivona *et al.* [33]. Moreover, the PE emission is due to the absorption and emission of an odd number of IR photons following one XUV photon absorption, whose photoionization line is absent in the PE spectrum. Hence, PE spectra in the perpendicular direction can hardly be observed for laser intensities lower than $10^{13}$ W/cm$^2$. Experimental measurements with strong lasers would be highly desirable in order to corroborate the present study. A recent work by Düsterer *et al.* [11] shows that they can be attainable now.

The paper is organized as follows: In Sec. II, we describe the semiclassical model (SCM) used to calculate the photoelectron spectra for the case of laser-assisted XUV ionization perpendicular to the polarization direction, which leads to simple analytical expressions. In Sec. III, we present the results and discuss the comparison of the SCM and the SFA outcomes and the *ab initio* calculation of the TDSE. Concluding remarks are presented in Sec. IV. Atomic units are used throughout the paper, except when otherwise stated.

## II. THEORY OF THE SEMICLASSICAL MODEL

We study the ionization of an atomic system interacting with an XUV pulse assisted by an IR laser. In the single-active-electron (SAE) approximation the TDSE reads

$$i \frac{\partial}{\partial t}|\psi(t)\rangle = [H_0 + H_{\text{int}}(t)]|\psi(t)\rangle, \qquad (1)$$

where $H_0 = \vec{p}^2/2 + V(r)$ is the time-independent atomic Hamiltonian, whose first term corresponds to the electron kinetic energy, and its second term to the electron-core Coulomb interaction. The second term in the right-hand side of Eq. (1), i.e., $H_{\text{int}} = \vec{r} \cdot \vec{F}_X(t) + \vec{r} \cdot \vec{F}_L(t)$, describes the interaction of the atom with both time-dependent XUV [$\vec{F}_X(t)$] and IR [$\vec{F}_L(t)$] electric fields in the length gauge.

The electron initially bound in the atomic state $|\phi_i\rangle$ is emitted with final momentum $\vec{k}$ and energy $E = k^2/2$ in the final state $|\phi_f\rangle$ belonging to the continuum. Then, the

photoelectron momentum distributions can be calculated as

$$\frac{dP}{d\vec{k}} = |T_{if}|^2, \qquad (2)$$

where $T_{if}$ is the $T$-matrix element corresponding to the transition $\phi_i \to \phi_f$.

Within the time-dependent distorted wave theory, the transition amplitude in the prior form and length gauge is expressed as

$$T_{if} = -i \int_{-\infty}^{+\infty} dt \, \langle \chi_f^-(\vec{r},t)|H_{\text{int}}(\vec{r},t)|\phi_i(\vec{r},t)\rangle, \qquad (3)$$

where $\phi_i(\vec{r},t) = \varphi_i(\vec{r})e^{iI_p t}$ is the initial atomic state, $I_p$ is the ionization potential, and $\chi_f^-(\vec{r},t)$ is the distorted final state [36,37]. The SFA neglects the Coulomb distortion in the final channel produced by the ejected-electron state due to its interaction with the residual ion. Hence, we can approximate the distorted final state with the Volkov function, which is the solution of the Schrödinger equation for a free electron in an electromagnetic field [38], i.e., $\chi_f^- = \chi_f^V$, where

$$\chi_f^V(\vec{r},t) = (2\pi)^{-3/2} \exp \left[ i(\vec{k} + \vec{A}(t)) \cdot \vec{r} \right.$$
$$\left. + \frac{i}{2} \int_t^\infty dt' (\vec{k} + \vec{A}(t'))^2 \right] \qquad (4)$$

and the vector potential due to the total external field is defined as $\vec{A}(t) = -\int_0^t dt'[\vec{F}_X(t') + \vec{F}_L(t')]$.

We consider the atomic photoionization due to a short XUV pulse assisted by an IR laser where both of them are linearly polarized in the same direction $\hat{z}$. For simplicity, we consider a hydrogen atom initially in the ground state, however, the present study can be easily generalized to any atom within the SAE approximation. In the present work, we restrict the photoelectron momentum $\vec{k} = k_z \hat{z} + k_\rho \hat{\rho}$ (in cylindrical coordinates) to the direction perpendicular to the polarization axis, i.e., $k_z = 0$ and $k_\rho \geqslant 0$. The case of emission parallel to the polarization axis, i.e., $k_\rho = 0$, was studied recently in [34].

With the appropriate choice of the IR and XUV laser parameters considered, we can assume that the energy domain of the LAPE processes is well separated from the domain of ionization by an IR laser alone. In other words, the contribution of IR ionization is negligible in the energy domain where the absorption of one XUV photon takes place. Besides, if we set the general expression of the XUV pulse of duration $\tau_X$ as $\vec{F}_X(t) = \hat{z}F_{X0}(t)\cos(\omega_X t)$, where $F_{X0}(t)$ is a slowly nonzero varying envelope function, the matrix element can be written as

$$T_{if} = -\frac{i}{2} \int_{t_0}^{t_0+\tau_X} dt \, d_z(\vec{k} + \vec{A}(t)) \, F_{X0}(t) \, e^{iS(t)} \qquad (5)$$

with $(t_0, t_0 + \tau_X)$ the temporal interval where $F_{X0}(t)$ is nonzero. $S(t)$ is the generalized action

$$S(t) = -\int_t^\infty dt' \left[ \frac{(\vec{k} + \vec{A}(t'))^2}{2} + I_p - \omega_X \right] \qquad (6)$$

and the $z$ component of the dipole element for the $1s$ state is

$$d_z(\vec{v}) = -\frac{i}{\pi} 2^{7/2} (2I_p)^{5/4} \frac{\hat{z} \cdot \vec{v}}{[v^2 + 2I_p]^3}. \quad (7)$$

In Eq. (5) we have used the rotating wave approximation which accounts, in this case, for the absorption of only one XUV photon and neglects, thus, the contribution of XUV photon emission. As the frequency of the XUV pulse is much higher than the IR laser one, the XUV contribution to the vector potential can be neglected [39,40], since the XUV intensity is not much higher than the laser one. For the sake of simplicity, we restrict our analysis to the case where the XUV pulse duration is a multiple of half the IR optical cycle, i.e., $\tau_X = NT_L = 2N\pi/\omega_L$, where $T_L$ and $\omega_L$ are the laser period and the frequency of the IR laser, respectively, and $2N$ is an integer positive number. During the temporal lapse that XUV pulse is present, the IR electric field can be modeled as a cosinelike wave, hence the vector potential can be written as $\vec{A}(t) = A_{L0} \sin(\omega_L t)\hat{z}$ with $A_{L0} = F_{L0}/\omega_L$ and $F_{L0}$ the amplitude of the laser electric field.

The SCM consists of solving the time integral Eq. (5) by means of the saddle-point approximation [41–44], wherein the transition amplitude can be thought of as a coherent superposition of the amplitudes of all electron classical trajectories with final momentum $\vec{k}$ over the stationary points $t_s$ of the generalized action $S(t)$ in Eq. (6),

$$T_{if} = \sum_{t_s} \frac{\sqrt{2\pi} \, F_{X0} \, d_z(\vec{k} + \vec{A}(t_s))}{|\ddot{S}(t_s)|^{1/2}}$$

$$\times \exp\left[ iS(t_s) + \frac{i\pi}{4} \text{sgn}(\ddot{S}(t_s)) \right], \quad (8)$$

where $\ddot{S}(t) = d^2 S(t)/dt^2 = -[\vec{k} + \vec{A}(t)] \cdot \vec{F}(t)$ and sgn denotes the sign function. Then, from the saddle-point equation, i.e., $\dot{S} = dS(t_s)/dt = 0$, the ionization times fulfill the relation

$$A^2(t_s) + k_\rho^2 = v_0^2, \quad (9)$$

where $v_0 = \sqrt{2(\omega_X - I_p)}$ is the initial velocity of the electron at the ionization time. In ionization by an IR laser alone, release times are complex due to the fact that the active electron escapes the core via tunneling through the potential barrier formed by the interaction between the core and the external field, i.e., $V(r) + \vec{r} \cdot \vec{F}_L(t)$. Contrarily, in LAPE, real solutions of Eq. (9) correspond to real ionization times $t_s$. From Eq. (9), the domain of allowed classical trajectories perpendicular to the polarization axis is $\sqrt{v_0^2 - A_{L0}^2} \leqslant k_\rho \leqslant v_0$ where $v_0 \geqslant F_{L0}/\omega_L$. Nonclassical trajectories with complex ionization times have a momentum $k_\rho$ outside the classical domain. In this work, we neglect the small weight of nonclassical trajectories with complex ionization times since its imaginary parts give rise to exponential decay factors.

The ionization times that verify Eq. (9) are shown schematically in Fig. 1 for one IR optical cycle. As we can observe, there are four ionization times per optical cycle and, therefore, the total number of interfering trajectories with the same final momentum perpendicular to the polarization axis is $4N$. A quick analysis of Eqs. (8) and (9) indicates that the periodicity for the solution of Eq. (9) is $\pi/\omega_L$, which is half of that
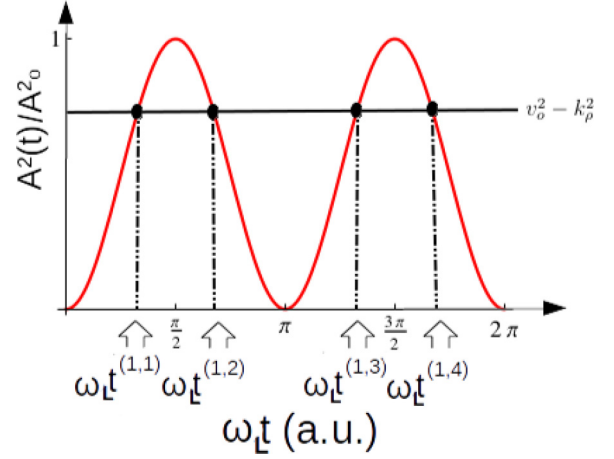


FIG. 1. Emission times (solutions of Eq. (9)) as the intersection of the two curves $A^2(t) = A_{L0}^2 \sin^2(\omega_L t)$ in red solid line and $v_0^2 - k_\rho^2$ in black solid line for one IR optical cycle. In this particular case, the XUV pulse starts when the potential vector vanishes.

corresponding to the parallel emission case [34]. Therefore, the sum over the emission times can be performed alternatively over $2N$ half cycles with two emission times in each of them. They are the early ionization time $t^{(m,1)}$ and the late ionization time $t^{(m,2)}$ corresponding to the $m$th optical half cycle, where $t^{(m,\beta)} = t^{(1,\beta)} + \pi(m-1)/\omega_L$ with $\beta = 1,2$. The expressions for the ionization times can be easily derived from Eq. (9),

$$t^{(1,1)} = \frac{1}{\omega_L} \sin^{-1}\left[ \sqrt{(v_0^2 - k_\rho^2)/A_{L0}^2} \right], \quad (10a)$$

$$t^{(1,2)} = \frac{\pi}{\omega_L} - t^{(1,1)}. \quad (10b)$$

From Eq. (6), the generalized action and its second derivative at the time $t_s$ for electron trajectories along the perpendicular direction can be written as

$$S(t_s) = \left( \frac{k_\rho^2}{2} + I_p + U_p - \omega_X \right) t_s - \frac{U_p}{2\omega_L} \sin(2\omega_L t_s) \quad (11)$$

and

$$\ddot{S}(t_s) = F_{L0} A_{L0} \sin(2\omega_L t_s)/2, \quad (12)$$

respectively, where $U_p = (F_{L0}/2\omega_L)^2$ is the ponderomotive energy of the oscillating electron driven by the laser field.

For the case of emission along the polarization axis in Ref. [34], the symmetry properties of the dipole matrix element were not taken into account since it can be factorized. Contrarily, for perpendicular emission they need to be considered since according to Eqs. (7) and (10), the dipole elements $d_z$ evaluated at emission times of consecutive half cycles differ in a sign, i.e.,

$$d_z(k_\rho \hat{\rho} + \hat{z} A(t^{(m,\beta)})) = \frac{\sqrt{2} A_{L0}}{i\pi \omega_X^3} \sin(\omega_L t^{(m,\beta)})$$

$$= -d_z(k_\rho \hat{\rho} + \hat{z} A(t^{(m+1,\beta)})). \quad (13)$$

Hence, the odd and even half cycles have opposite contributions. Including Eqs. (10) and (13) into Eq. (8), the ionization

probability of Eq. (2) can be written as

$$|T_{if}|^2 = \Gamma(k_\rho) \left| \sum_{m=1}^{2N} \sum_{\beta=1}^{2} (-1)^m \exp\left[ i S(t^{(m,\beta)}) + \frac{i\pi}{4} \text{sgn}(\ddot{S}(t^{(m,\beta)})) \right] \right|^2. \tag{14}$$

Equation (14) can be interpreted as the coherent sum over interfering trajectories decomposed into those associated with the two release times within the same half cycle (inner summation) and those associated with release times in the $2N$ different half cycles (outer summation). The ionization probability $\Gamma(k_\rho)$ contains all identical factors for all subsequent ionization trajectories which depend on the final momentum $k_\rho$, i.e.,

$$\Gamma(k_\rho) = \frac{4F_{X0}^2}{\pi \omega_X^6 \omega_L} \frac{\sqrt{v_0^2 - k_\rho^2}}{\sqrt{k_\rho^2 - v_0^2 + A_{L0}^2}}. \tag{15}$$

In the same way as in previous works [34,45,46] and after a bit of algebra, it can be shown that

$$\sum_{m=1}^{2N} \sum_{\beta=1}^{2} (-1)^m \ e^{\left[ i S(t^{(m,\beta)}) + (i\pi/4)\text{sgn}(\ddot{S}(t^{(m,\beta)})) \right]}$$

$$= 2 \sum_{m=1}^{2N} e^{i(\bar{S}_m + m\pi)} \cos\left( \frac{\Delta S_m}{2} + \frac{\pi}{4} \right), \tag{16}$$

where $\bar{S}_m = [S(t^{(m,1)}) + S(t^{(m,2)})]/2 = S_0 + m(\tilde{S}/2)$ is the average action of the two trajectories released in the $m$th half cycle, with $\tilde{S} = (2\pi/\omega_L)(E + I_p + U_p - \omega_X)$ and $S_0$ an unimportant constant that will be canceled out when the absolute value is taken in Eq. (14). The accumulated action between the two release times $t^{(m,1)}$ and $t^{(m,2)}$ within the same $m$th half cycle, $\Delta S_m = S(t^{(m,1)}) - S(t^{(m,2)})$ in Eq. (16), is given by

$$\Delta S = \frac{\tilde{S}}{2} \left\{ \frac{2}{\pi} \sin^{-1}\left[ \sqrt{(v_0^2 - k_\rho^2)/A_{L0}^2} \right] - 1 \right\}$$

$$- \frac{1}{2\omega_L} \sqrt{v_0^2 - k_\rho^2} \sqrt{k_\rho^2 - v_0^2 + A_{L0}^2}, \tag{17}$$

where we have omitted the subscript $m$, since it is independent of which half cycle is considered. It is worthwhile to note that the expression of the accumulated action in Eq. (17) differs from the one for parallel emission [see Eq. (22) in Ref. [34]]. Finally, due to the linear dependence of the average action $\bar{S}_m$ on the cycle number $m$ and the factorization of the cosine factor in the right-hand side of Eq. (16), the ionization probability can be easily written as

$$|T_{if}|^2 = 4\Gamma(k_\rho) \underbrace{\cos^2\left( \frac{\Delta S}{2} + \frac{\pi}{4} \right)}_{\text{intra-half-cycle}} \underbrace{\left[ \frac{\sin(N\tilde{S}/2)}{\cos(\tilde{S}/4)} \right]^2}_{\text{inter-half-cycle}}. \tag{18a}$$

$$= 4\Gamma(k_\rho) \underbrace{4\cos^2\left( \frac{\Delta S}{2} + \frac{\pi}{4} \right) \sin^2\left( \frac{\tilde{S}}{4} \right)}_{\text{intracycle}} \underbrace{\left[ \frac{\sin(N\tilde{S}/2)}{\sin(\tilde{S}/2)} \right]^2}_{\text{intercycle}}. \tag{18b}$$

Equations (18a) and (18b) indicate that the photoelectron spectrum can be factorized in two different ways. (i) On one hand, the factorization in Eq. (18a) highlights the contribution of the pair of electron trajectories within the same half cycle (intra-half-cycle interference), governed by the factor $G(k_\rho) = \cos^2(\Delta S/2 + \pi/4)$, and the interference stemming from trajectories released at different half cycles (inter-half-cycle interference) described by the factor $H(k_\rho) = [\sin(N\tilde{S}/2)/\cos(\tilde{S}/4)]^2$. On the other hand, the factor $F(k_\rho) = 4\cos^2(\Delta S/2 + \pi/4)\sin^2(\tilde{S}/4)$ stems from the contribution of the four trajectories within the same optical cycle (intracycle interference), and the factor $B(k_\rho) = \sin^2(N\tilde{S}/2)/\sin^2(\tilde{S}/2)$ stems from trajectories released at different cycles (intercycle interference, in correspondence with previous analysis of Eq. (23) in [34]). Whereas in (i) the interference of $2N$ half cycles is highlighted giving rise to the intra-half- and inter-half-cycle factors, in (ii) we think of the coherent contributions of $N$ different optical cycles splitting the contribution in intra- and intercycle interference patterns. Obviously, the two different factorizations give rise to the same results, i.e., $G(k_\rho)H(k_\rho) = F(k_\rho)B(k_\rho)$.

In Fig. 2(a), we plot the intra-half-cycle function $G(k_\rho)$ and the inter-half-cycle $H(k_\rho)$ for a XUV laser pulse duration $\tau_X = 2T_L$ as a function of the energy. Whereas the intra-half-cycle factor $G(k_\rho)$ exhibits a nonperiodic oscillation, the inter-half-cycle $H(k_\rho)$ is periodic in the final photoelectron energy with peaks at positions $E_\ell = k_\rho^2/2$ given by

$$E_\ell = \omega_X + (2\ell + 1)\omega_L - I_p - U_p \tag{19}$$

with $\ell = \ldots, -2, -1, 0, 1, 2, \ldots$. In fact, in the limit of infinitely long XUV and IR pulses, $\lim_{N\to\infty} H(k_\rho) = \sum_l \delta(\tilde{S}/4 + \pi/2 - \ell\pi)$, the ionization probability vanishes unless the final energy satisfies Eq. (19) which gives the positions of the different sidebands. We see that the energy difference between two consecutive sidebands is $2\omega_L$ and not $\omega_L$ as for the emission in the direction parallel to the polarization axis [34]. From Eq. (19), it is easy to see that only odd numbers $(2\ell + 1)$ of laser photons can be absorbed or emitted together with the absorption of one XUV photon. Due to the lack of sidebands for the absorption or emission of an even number of laser photons, the absorption of only one XUV photon alone (in the absence of absorption or emission of IR photons) is forbidden. The intra-half-cycle pattern displays few oscillations with maxima depending on the electron kinetic energy. These can be easily calculated through $\Delta S = (2q - 1/2)\pi$, with integer $q$. In Fig. 2(b), we plot the total interference pattern corresponding to an XUV pulse of duration $\tau_X = 2T_L$, and the intracycle factor $F(k_\rho)$. For the sake of comparison, we reproduce in Fig 2(b) the intra-half-cycle factor $G(k_\rho)$ of Fig. 2(a). All interference factors have been rescaled for better visualization. The multiplication of both intra-half-cycle and inter-half-cycle factors, i.e., $G(k_\rho)H(k_\rho)$, is displayed in Fig. 2(b), where we observed
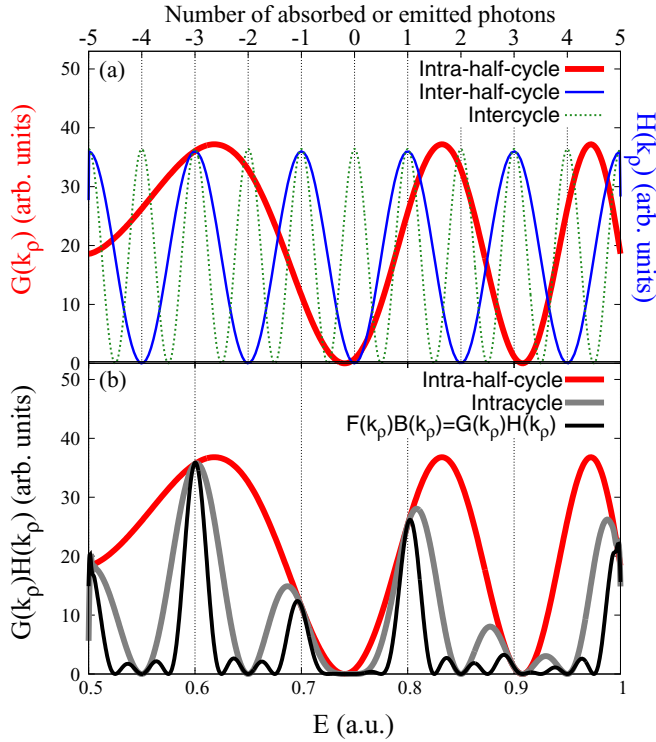
FIG. 2. Buildup of the interference pattern following the SCM for $N = 2$. (a) Intra-half-cycle interference pattern given by $G(k_\rho)$ in thick red line, intercycle pattern given by the factor $B(k_\rho)$ in thin dotted green (light grey) line and inter-half-cycle pattern given by the factor $H(k_\rho)$ in thin blue (grey) line. (b) Intracycle pattern given by the factor $F(k_\rho)$ in thick gray line and total interference pattern $F(k_\rho)B(k_\rho) = G(k_\rho)H(k_\rho)$ in thin black line. Vertical lines depict the positions of the sidebands $E_\ell$ of Eq. (19). The IR laser parameters are $F_{L0} = 0.05$, and $\omega_L = 0.05$, and the XUV frequency is $\omega_X = 1.5$.

how the intra-half-cycle interference pattern [$G(k_\rho)$] works as a modulation of the intracycle interference pattern [$F(k_\rho)$] and the latter does the same with the sidebands (intercycle interference pattern). Small deviations of the different maxima of the intracycle interference pattern in Fig. 2(b) with respect to the conservation of energy in Eq. (19) can be easily observed. The width of the peaks is involved in the explanation of these small deviations: For the intracycle distribution ($\tau_X = T_L$), the factor $H(k_\rho)$ in Eq. (18a) is responsible for the sidebands centered at $E_\ell$ [in agreement with Eq. (19)] and widths equal to $\Delta E = 2\omega_L/N$. The intra-half-cycle envelope factor $G(k_\rho)$ modulates the factor $H(k_\rho)$ shifting slightly the peaks, i.e., for energies where $G(k_\rho)$ is an increasing function the peaks shift to the right (higher energies), whereas where $G(k_\rho)$ is a decreasing function they move to the left. As the XUV pulse gets longer, i.e., $N$ is higher, the sidebands are sharper and the peaks shift less. As pointed out before, in the limit $N \gg 1$, the sidebands became $\delta$ functions and, thus, they do not move with the intra-half-cycle envelope.

On the other hand, Eq. (18b) shows that the photoelectron spectrum can be thought of as the intercycle pattern with peaks at positions $E_n = n\omega_L + \omega_X - I_p - U_p$ modulated by the intracycle interference pattern given by the factor $F(k_\rho)$. Therefore, the lack of even-order sidebands stems from the

factor $\sin^2(\tilde{S}/4)$ into the intracycle factor $F(k_\rho)$ [see Eq. (18a)]. The factor $\sin^2(\tilde{S}/4)$ reflects the fact that the dipole element has opposite signs for the two different half cycles into the same optical cycle [see Eq. (13)] giving rise to destructive interference between the contribution of the two electron trajectories of the first half cycle with the corresponding to the second half cycle of every optical cycle during the time interval that the XUV pulse is on. Contrarily, for emissions in the parallel direction, whereas the ionization during one of the two half cycles contributes to emissions in one direction (forward or backward), the other half cycle will contribute to the opposite direction [34]. Therefore, no interference is produced for parallel emissions allowing to all peaks separated by $\omega_L$.

## III. RESULTS AND DISCUSSION

We need to compare the outcome of SCM calculations with quantum ones in order to probe the general conclusion of the SCM: The ionization probability of electrons emitted perpendicularly to the polarization axis of the XUV and the laser pulse can be factorized in two different contributions in two different ways: (i) intra-half-cycle and inter-half-cycle interferences [Eq. (18a)] and (ii) intracycle and intercycle interferences [Eq. (18b)]. We have performed calculations within the SFA and TDSE methods, which have been extensively covered in the literature and in our previous work [34] and we do not repeat them here. For the SFA calculating method, please refer, for example, to Refs. [31–33,37,45,46], and for the *ab initio* numerical solutions of the TDSE we employ the generalized pseudospectral method combined with the split-operator representation of the time-evolution operator, which is thoroughly explained in the literature (see, for example, [47–49]). For the computational feasibility of the SFA and TDSE calculations, we take the XUV pulse and the IR laser field modeled as

$$\vec{F}_i(t) = F_{i0}(t - t_{ib}) \cos\left[\omega_i\left(t - \Delta_i - \frac{\tau_L}{2}\right)\right]\hat{z}, \quad (20)$$

where $i = L$ and $X$ denote the IR laser and XUV pulses, respectively. The envelopes of the electric fields in Eq. (20) were chosen as

$$F_{i0}(t) = F_{i0}\begin{cases} t/T_i & \text{if} \quad 0 \leqslant t \leqslant T_i \\ 1 & \text{if} \quad T_i \leqslant t \leqslant \tau_i - T_i \quad (21) \\ (\tau_i - t)/T_i & \text{if} \quad \tau_i - T_i \leqslant t \leqslant \tau_i \end{cases}$$

and zero otherwise, where $T_i = 2\pi/\omega_i$ and $\tau_i$ are the $i$-field period and pulse duration, respectively. It describes a central flattop region and linear one-cycle ramp on and ramp off. For the sake of simplicity, we suppose that the duration of both laser fields comprise an integer number of cycles, i.e., $\tau_i = N_i T_i$ where $N_i$ is a positive integer. In addition, as we have mentioned before, we also consider the case where $\tau_X = NT_L$. We choose the origin of the time scale as the beginning of the IR laser pulse, i.e., $t_{Lb} = 0$, with no displacement of the laser pulse $\Delta_L = 0$. In this way, the IR laser field is a cosinelike pulse centered in the middle of the pulse, $t = \tau_L/2$. In Eq. (20), the time delay of the XUV pulse with respect to the laser pulse is $\Delta_X$ and $t_{Xb} = \Delta_X + \tau_L/2 - \tau_X/2$ denotes the
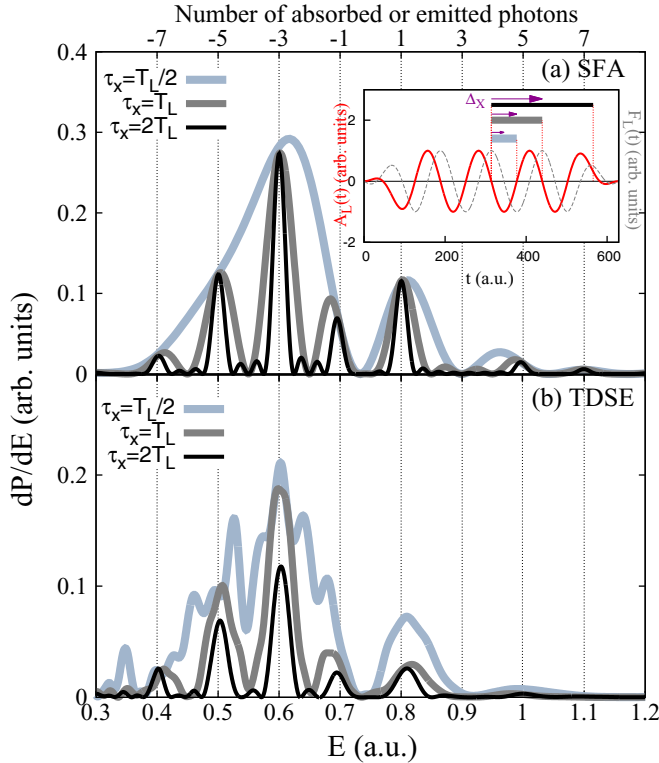
FIG. 3. Photoelectron spectra in the perpendicular direction calculated within (a) the SFA and (b) the TDSE, for different XUV pulse durations $\tau_X = T_L/2$ (thick light gray), $T_L$ (thick gray), and $2T_L$ (thin black) and respective time delays $\Delta_X = T_L/4$, $T_L/2$, and $T_L$. The XUV and IR parameters are the same as in Fig. 2 and $\tau_L = 5T_L$ and $F_{X0} = 0.05$. Vertical lines depict the positions of the sidebands according to Eq. (19). The photoelectron energy distributions have been rescaled for better visualization.

beginning of the XUV pulse that depends on the XUV pulse duration. It also marks the starting time of the active window for ionization. The vector potential from the perspective of the active window is shifted when comparing different XUV pulse durations due to the different values of $t_{Xb}$. Therefore, for the sake of comparison of the ionization yield for different XUV pulse durations, the active window should be in phase with the vector potential. For that, we define the module $2\pi$ optical phase $\phi \equiv \omega_L t_{Xb} = \omega_L \Delta_X + (N_L - N)\pi$ as the phase of the starting time of the XUV pulse with respect to the vector potential $\vec{A}(t)$ [50].

In the following, we probe the results of the SCM by comparing the photoelectron spectrum $dP/dE = 2\pi \sqrt{2E} |T_{if}|^2$ to quantum simulations. We consider the IR and XUV frequencies as $\omega_L = 0.05$ and $\omega_X = 30\omega_L = 1.5$ respectively, the IR laser duration $\tau_L = 5T_L$, and three different XUV pulses with durations $\tau_X = T_L/2$, $T_L$, and $2T_L$ (i.e., $N = 1/2$, 1, and 2). For these parameters, the SCM and SFA estimates ratios between transversal and forward emission of about 4% and 2%, respectively, the latter in agreement with the TDSE prediction. In Figs. 3 and 4 we consider the corresponding time delays $\Delta_X = T_L/4$, $T_L/2$, and $T_L$, so that the optical phases are the same $\phi = \pi$. In Fig. 3(a) and 3(b) we show results of the SFA and the numerical solution of the TDSE, respectively, for

the same XUV and IR pulse parameters used in Fig. 2 with $F_{X0} = F_{L0} = 0.05$. The agreement among the SCM (Fig. 2), the SFA (Fig. 3(a)), and TDSE [Fig. 3(b)] energy distributions is very good since the effect of the Coulomb potential on the energy spectrum for electron emission in the perpendicular direction is very small if not negligible. However, the analysis of the effect of the Coulomb potential of the remaining core on the electron yield deserves a thorough study, which is beyond the scope of this paper. As predicted in Eq. (18a), the intra-half-cycle interference pattern, calculated as the energy distribution for a XUV pulse duration of half a laser cycle, i.e., $\tau_X = T_L/2$, modulates the intracycle interference pattern, calculated as the energy distribution for a XUV pulse duration of one laser cycle, i.e., $\tau_X = T_L$. In the same way, the latter modulates the sidebands in the energy distribution for a longer XUV pulse, i.e., $\tau_X = 2T_L$, as shown in Figs. 3(a) and 3(b). For the latter case (when the XUV pulse duration involves several periods of the laser, i.e., $\tau_X = 2T_L$), the positions of the sidebands obtained by the quantum calculations (SFA and TDSE) in Figs. 3(a) and 3(b) agree with the SCM expressed in Eq. (19). As expected, the energy spectra for the quantum SFA and TDSE calculations extend beyond the classical limits $E_{low} = v_0^2/2 - 2U_p = 0.5$ and $E_{up} = v_0^2/2 = 1$. The TDSE spectrum for the shorter XUV duration case in Fig. 3(b) presents several additional structures that are related to the direct electronic emission due to the IR laser only. This is discussed in the context of the next figure.

We have investigated the dependence of the energy distribution for photoelectrons emitted in the direction perpendicular to the polarization axis on the intensity of the XUV pulse. We have checked that the total (angle- and energy-integrated) ionization probability is essentially proportional to the intensity of the XUV pulse whereas the overall shape of the energy distribution in the transversal direction (Fig. 3) remains rather unchanged when varying the intensity of the XUV pulse (not shown). Contrarily, the intensity of the IR laser has a strong effect on the shape of the energy distribution. In Fig. 4 we show calculations of the energy distribution in the perpendicular direction within the SCM in (a), (d), and (g), the SFA in (b), (e), and (h), and the TDSE in (c), (f), and (i), for laser field intensities from $I_L = 0$ up to $8.8 \times 10^{13}$ W/cm² ($F_{L0} = 0.05$). We analyze the energy distribution for different XUV pulse durations. The energy spectra for $\tau_X = T_L/2$, $T_L$, and $2T_L$ in Figs. 2 and 3 are cuts of Fig. 4 at $I_L = 8.8 \times 10^{13}$ W/cm². The classical boundaries $E_{low}$ and $E_{up}$ drawn in dotted lines exactly delimit the SCM spectrogram of Figs. 4(a), 4(d) and 4(g), as expected. For the case where $\tau_X = T_L/2$ (first column), Figs. 4(a)–4(c) show a negative slope of the intra-half-cycle interference stripes. The value of the slope for the maxima can be calculated numerically from the transcendental equation for the energy $\Delta S = (2q - 1/2)\pi$ with $q = -2, -1, 1, 2, \ldots$ [see Eq. (17)]. For the cases $\tau_X = T_L$ (second column of Fig. 4), we observed in Figs. 4(d)–4(f) that the intra-half-cycle interference patterns are flanked by stripes of zero or near zero probability distribution corresponding to the zeros of the factor $\sin(\tilde{S}/4)$ in the intracycle factor $F(k_\rho)$, i.e., $\tilde{S}/4 = n\pi$, which gives $E = \omega_X - I_p - U_p + 2n\omega_L$. The slope of these minima is $-U_p/I_L = -(2\omega_L)^{-2}$ and the energy difference between consecutive minima (and maxima) is $2\omega_L$. For the case of $\tau_X = 2T_L$ (third column of Fig. 4), we see in Figs. 4(g)–4(i) that the
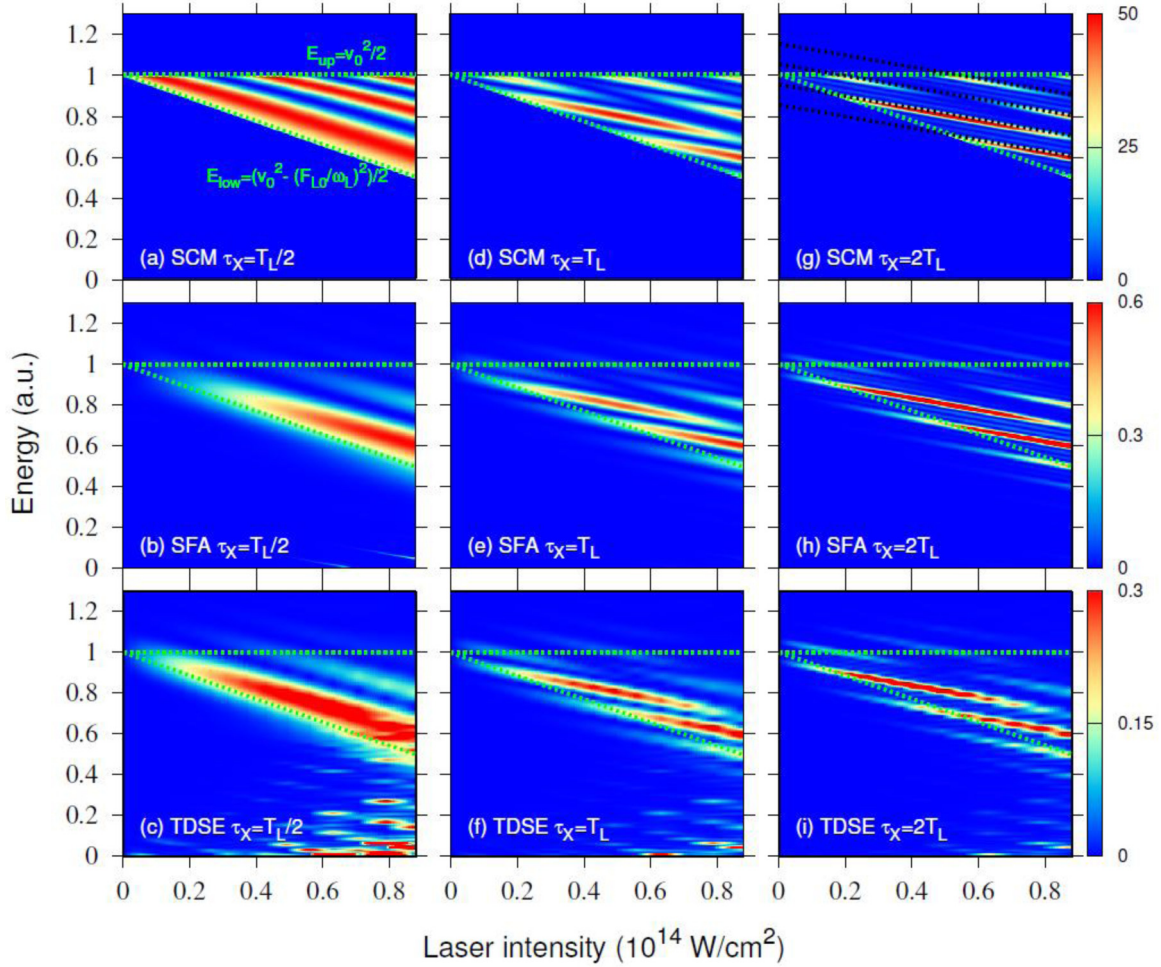
FIG. 4. Photoelectron spectra in the perpendicular direction (in arbitrary units) calculated at different laser field strengths within the SCM [(a), (d), and (g)], the SFA [(b), (e), and (h)], and the TDSE [(c), (f), and (i)]. The XUV pulse durations are $\tau_X = T_L/2$ [(a)–(c)], $\tau_X = T_L$ [(d)–(f)], and $\tau_X = 2T_L$ [(g)–(i)]. The other XUV and IR parameters as in previous figures. In green dotted line we show the classical boundaries and in black dotted line the $E_\ell$ values given by Eq. (19). The photoelectron energy distributions have been rescaled for better visualization.

stripes of the probability distribution become even thinner due to the effect of the destructive inter-half-cycle interference for energy values much different than the conservation energy for absorption of one XUV photon and an odd number of IR laser photons [Eq. (19)]. Moreover, when we compare the position of the maxima with Eq. (19), marked as black dotted lines in Fig. 4(g), we see an excellent agreement (see also Fig. 3). The domain of the SFA and TDSE spectrograms (second and third rows of Fig. 3) extend beyond the classical boundaries with smooth edges. The characteristic intra-half- and intracycle stripes with negative slope reproduce very well the SCM predictions.

In Figs. 4(c), 4(f) and 4(i), the TDSE calculations exhibit a strong probability distribution for high values of the laser intensity $I_L \gtrsim 0.5 \times 10^{14}$ W/cm$^2$ in the low-energy region which almost does not overlap with the laser assisted XUV ionization for the longer XUV duration cases, but for the $\tau_X = T_L/2$ case. We suspect that these structures are responsible for those appearing in Fig. 3(b). The source of this probability enhancement is the atomic ionization by the IR laser pulse alone, which has not been considered in our SCM and is strongly suppressed in the SFA because the laser photon energy

is much lower than the ionization potential, i.e., $\omega_L \ll I_p$. For this reason, we can confirm that the SFA is a more reliable method to deal with laser assisted photoemission compared to ATI by IR lasers [34]. Therefore, except for the region where ionization by the laser field alone becomes important, SFA and TDSE spectrograms exhibit a very good agreement between them and resemble the SCM calculations qualitatively well. The resulting energy stripes become thinner and more pronounced as the duration of the XUV pulse increases, exhibiting the fact that the intra-half-cycle interference pattern modulates the intracycle pattern, which, at the same time, modulates the sidebands (intercycle interference pattern). We rescale the photoelectron spectra in Figs. 4(c), 4(f) and 4(i) with factors 1:1, 1:2, and 1:4, respectively, in order to keep the (intra-half-, intracycle, and intercycle) LAPE interferences comparable since the ionization yield scales with the pulse duration. By varying the XUV pulse duration the near-threshold structures should be unaltered and this is essentially what we observe from our TDSE computations. However, due to the rescaling factors, one sees that the low-energy structures decrease as the XUV pulse gets longer. The right way to see this is that the relative importance of the IR contribution to the
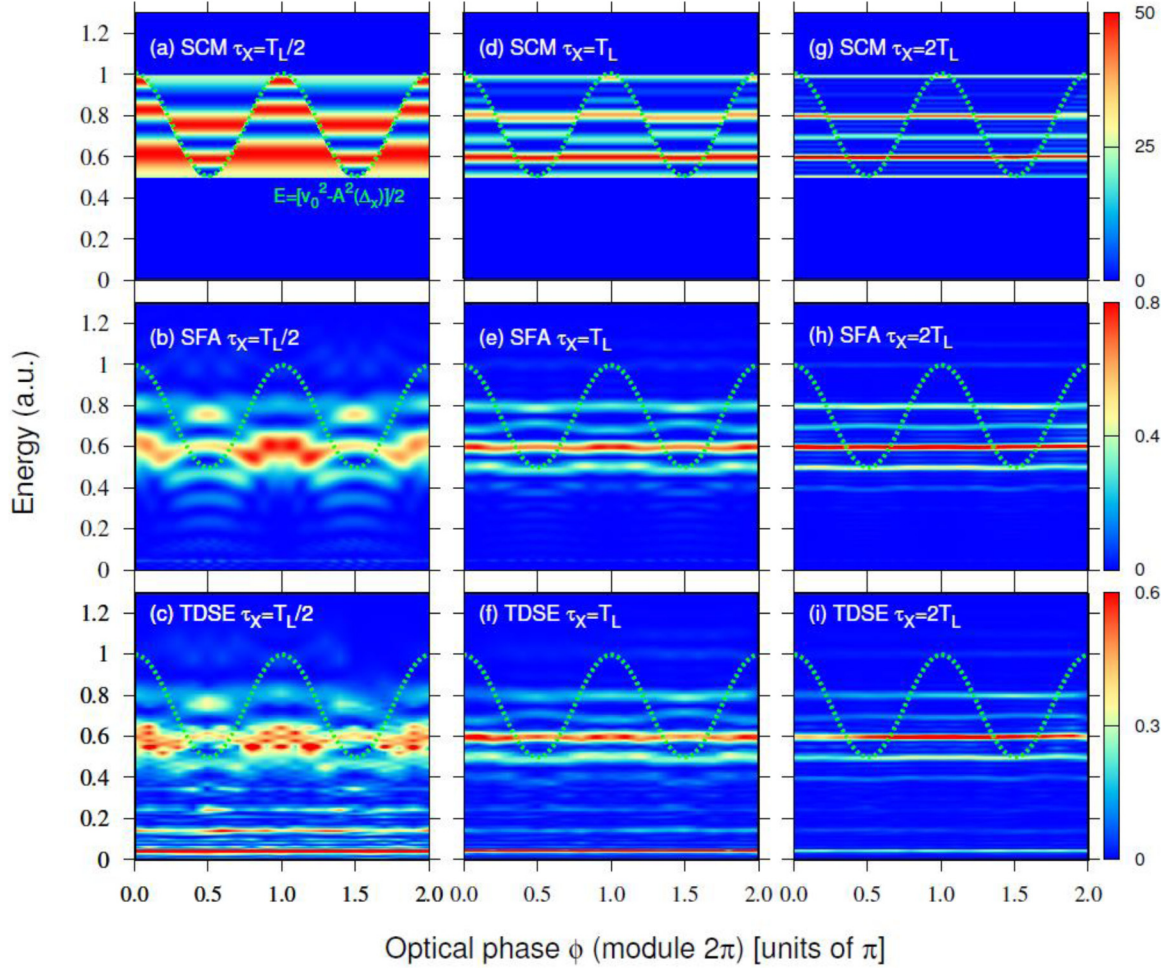
FIG. 5. Photoelectron spectra in the perpendicular direction (in arbitrary units) calculated as a function of the time delay $\Delta_X$ within the SCM [(a), (d), and (g)], the SFA [(b), (e), and (h)], and the TDSE [(c), (f), and (i)]. The XUV pulse durations are $\tau_X = T_L/2$ [(a)–(c)], $\tau_X = T_L$ [(d)–(f)], and $\tau_X = 2T_L$ [(g)–(i)]. The other XUV and IR parameters as in previous figures. In dotted line we show the energy values of Eq. (22). The photoelectron energy distributions have been rescaled for better visualization.

whole ionization yield (LAPE) diminishes as the XUV pulse duration is higher.

So far, we have performed our analysis of the electron emission in the transverse direction for optical phase $\phi = \pi$ (since $N_L$ is odd). In order to reveal how the intracycle interference pattern changes with the time delay, we vary $\Delta_X$ in an optical cycle, so that $\phi$ varies from 0 to $2\pi$. In Fig. 5(a) we show the intra-half-cycle interference pattern calculated for $\tau_X = T_L/2$ within the SCM in the transverse direction as a function of the optical phase module $2\pi$. The horizontal stripes show the independence of the intra-half-cycle interference pattern with the time delay, except for the discontinuity for energy values equal to

$$E_{\text{disc}} = \tfrac{1}{2}\big[v_0^2 - A^2(t_{Xb})\big]. \qquad (22)$$

For $\phi = 0$ the discontinuity is situated at $E_{\text{disc}} = v_0^2/2$ [since in this case $\Delta_X = 3T_L/4$ for $N = 1/2$ and then $A(t_{Xb} = 3T_L) = 0$], which coincides with the classical boundary. Figure 5(a) shows us that as $\phi$ (and $\Delta_X$) varies, the discontinuity follows the shape of the square of the vector potential, which means that the discontinuity is $\pi$ periodic in $\phi$, contrarily to the

$2\pi$ periodicity in the case of parallel emission [34]. For phase values $\phi = 0$, $\pi$, and $2\pi$, the discontinuity situates at $E_{\text{up}} = v_0^2/2 = 1$, whereas for $\phi = \pi/2$ and $3\pi/2$, it does at $E_{\text{low}} = v_0^2/2 - 2U_p = 0.5$, losing entity in both cases. The SFA and TDSE energy distributions, in the respective Figs. 5(b) and 5(c), exhibit similar characteristics to the SCM, but with a richer $\pi$-periodic structure. Interestingly, the discontinuity at $E_{\text{disc}}$ is reflected as a jump of the probability distributions for the same energy values. The remarkable resemblance between the computationally cheap SFA and the *ab initio* solution of the TDSE results shows, once again, that the SFA is very appropriate to explain and reproduce the electron yield in LAPE processes. Low-energy contributions in TDSE calculations shown in Fig. 5(a) are due to IR ionization as described before in Figs. 4(c)–4(e).

For $\tau_X = T_L$ in Fig. 5(d), the SCM spectrum displays horizontal lines corresponding to the intracycle interference or, what is the same, to the interplay between the intra-half-cycle factor $G(k_\rho)$ and the factor $\sin^2(\tilde{S}/4)$, according to Eq. (18b). In the same way, for the case where $\tau_X = 2T_L$ in Fig. 5(g) the SCM spectrum displays horizontal lines corresponding to the intercycle interference modulated by

the intracycle pattern of Fig. 5(d). We note that there is no discontinuity in the factor $G(k_\rho)$ at the energy values $E_\ell$ given by Eq. (19). Hence, as the sidebands get narrower, discontinuity of the intracycle modulation blurs. Continuity in the intracycle and intra-half-cycle factors is related to the fact that the accumulated action at both sides of the discontinuity verifies that $\Delta S|_{E > E_{\mathrm{disc}}} + \Delta S|_{E < E_{\mathrm{disc}}} = \tilde{S}/2$, where $\Delta S|_{E > E_{\mathrm{disc}}}$ ($\Delta S|_{E < E_{\mathrm{disc}}}$) is the accumulated action calculated at energies higher (lower) than the discontinuity $E_{\mathrm{disc}}$. Hence, the evaluation of $\cos^2(\Delta S/2 + \pi/4)$ gives exactly the same result at $E_\ell$ independently on $\phi$. Once more, from the SFA spectrograms displayed in Figs. 5(e) and 5(h) and the corresponding TDSE calculations in Figs. 5(f) and 5(i), we can see, once again, that the agreement between the SFA and TDSE spectrograms is very good, with the exception of a contribution at low energies due to the ionization by the IR laser pulse alone, which is strongly suppressed in the SFA calculations. By comparing the intra-half-cycle pattern for $\tau_X = T_L/2$ in the left column [Figs. 5(a)–5(c)] to the intracycle interference pattern in $\tau_X = T_L$ in the center column [Figs. 5(d)–5(f)] and the whole interference pattern for $\tau_X = 2T_L$ in the right column [Figs. 5(g)–5(i)], we corroborate the SCM prediction that the intra-half-cycle interference pattern (spectrogram for $\tau_X = T_L/2$) works as a modulator of the intracycle pattern (spectrogram for $\tau_X = T_L$), whereas the latter does the same with the intercycle interference pattern or sidebands.

## IV. CONCLUSIONS

We have studied the electron emission produced by atomic hydrogen in its ground state subject to an XUV pulse in the presence of an infrared laser pulse in the direction perpendicular to the common polarization axis of both pulses. The previously developed SCM [34] for LAPE (XUV + IR) in the forward direction has been reformulated for perpendicular emission. The goodness of our model over others is more evident for emission in the perpendicular emission. Few theoretical approaches are mentioned in the literature: soft-photon approximation [14], Kazansky's first-order time-dependent perturbation theory [21,22,31,32], and Bivona's theory [33]. Whereas the first two predict null perpendicular emission for ionization from an *s* state, only the last one foresees nonzero perpendicular probability. Our study not only agrees with the latter, but also goes beyond by analyzing the properties of perpendicular emission much more thoroughly. In accordance to our recent study of LAPE in the forward direction [34], the PE spectrum can be factorized as two contributions: One accounting for sidebands formation and the other as a modulation. Whereas the former can be interpreted as the

intercycle interference of electron trajectories from different optical cycles of the IR laser, the latter corresponds to intracycle interference stemming from the coherent superposition of four electron trajectories born in the same optical cycle. Contrary to parallel emission, the intracycle interference pattern for transversal emission can be decomposed as the contribution of the two interfering trajectories born within the same half optical period (intra-half-cycle interference) and the Young-type interference between the contributions of the two half cycles into the same optical cycle (inter-half-cycle interference). We have shown that the electron trajectories born into the two half cycles within the same optical cycle interfere destructively for the absorption and/or emission of an even number of IR photons, which leads to the exchange of only an odd number of laser photons in the formation of the sidebands. Therefore, the absorption line of the XUV photon alone (with no exchange of laser photons) is forbidden. We show that the intra-half-cycle interference pattern modulates the intracycle pattern, which, in the same way, modulates the sidebands. We have observed a very good agreement of our SCM energy spectrum with the corresponding one to the SFA and the *ab initio* solution of the TDSE.

We have observed that as the laser intensity increases the spectra becomes wider and approximately bounded within the classical energy domain. Another difference between the emission parallel and perpendicular to the polarization axis is the classical boundaries. We have shown that the upper energy boundary in perpendicular emission is independent of the laser intensity, contrary to parallel emission which increases linearly with energy [34]. In turn, the lower classical boundaries in both cases increases as the laser intensity grows, but at different rates. The values of these boundaries can be useful to know the elusive magnitude of the laser intensity in experiments. We can conclude that the SFA is accurate to describe the PE spectrum perpendicular to the polarization direction, especially for low and moderate laser intensities so that the electron ionization by the IR laser alone is low compared to LAPE. Finally, by analyzing the electron spectrum as a function of the time delay between the two pulses $\Delta_X$, we have shown that the intra-half-cycle pattern is $\pi$ periodic in the optical phase with a probability jump that reproduces the profile of the square of the laser vector potential.

[1] V. Véniard, R. Taïeb, and A. Maquet, Phys. Rev. Lett. **74**, 4161 (1995).

[2] T. E. Glover, R. W. Schoenlein, A. H. Chin, and C. V. Shank, Phys. Rev. Lett. **76**, 2468 (1996).

[3] S. A. Aseyev, Y. Ni, L. J. Frasinski, H. G. Muller, and M. J. J. Vrakking, Phys. Rev. Lett. **91**, 223902 (2003).

[4] P. O'Keeffe, R. López-Martens, J. Mauritsson, A. Johansson, A. L'Huillier, V. Véniard, R. Taïeb, A. Maquet, and M. Meyer, Phys. Rev. A **69**, 051401 (2004).

[5] O. Guyétand, M. Gisselbrecht, A. Huetz, P. Agostini, R. Taïeb, V. Véniard, A. Maquet, L. Antonucci, O. Boyko, C. Valentin, and D. Douillet, J. Phys. B: At., Mol. Opt. Phys. **38**, L357 (2005).

[6] M. Meyer, D. Cubaynes, D. Glijer, J. Dardis, P. Hayden, P. Hough, V. Richardson, E. T. Kennedy, J. T. Costello, P. Radcliffe, S. Düsterer, A. Azima, W. B. Li, H. Redlin, J. Feldhaus, R. Taïeb, A. Maquet, A. N. Grum-Grzhimailo, E. V. Gryzlova, and S. I. Strakhova, Phys. Rev. Lett. **101**, 193002 (2008).

[7] M. Meyer, J. T. Costello, S. Düsterer, W. B. Li, and P. Radcliffe, J. Phys. B: At., Mol. Opt. Phys. **43**, 194006 (2010).

[8] P. Radcliffe, M. Arbeiter, W. B. Li, S. Düsterer, H. Redlin, P. Hayden, P. Hough, V. Richardson, J. T. Costello, T. Fennel, and M. Meyer, New J. Phys. **14**, 043008 (2012).

[9] T. Mazza, M. Ilchen, A. J. Rafipoor, C. Callegari, P. Finetti, O. Plekan, K. C. Prince, R. Richter, M. B. Danailov, A. Demidovich, G. De Ninno, C. Grazioli, R. Ivanov, N. Mahne, L. Raimondi, C. Svetina, L. Avaldi, P. Bolognesi, M. Coreno, P. O'Keeffe *et al.*, Nat. Commun. **5**, 3648 (2014).

[10] P. Hayden, J. Dardis, P. Hough, V. Richardson, E. T. Kennedy, J. T. Costello, S. Düsterer, H. Redlin, J. Feldhaus, W. B. Li, D. Cubaynes, and M. Meyer, J. Mod. Opt. **63**, 358 (2016).

[11] S. Düsterer, G. Hartmann, F. Babies, A. Beckmann, G. Brenner, J. Buck, J. Costello, L. Dammann, A. D. Fanis, P. Geßler, L. Glaser, M. Ilchen, P. Johnsson, A. K. Kazansky, T. J. Kelly, T. Mazza, M. Meyer, V. L. Nosik, I. P. Sazhina, F. Scholz, J. Seltmann, H. Sotoudi, J. Viefhaus, and N. M. Kabachnik, J. Phys. B: At., Mol. Opt. Phys. **49**, 165003 (2016).

[12] R. Kienberger, M. Hentschel, M. Uiberacker, C. Spielmann, M. Kitzler, A. Scrinzi, M. Wieland, T. Westerwalbesloh, U. Kleineberg, U. Heinzmann, M. Drescher, and F. Krausz, Science **297**, 1144 (2002).

[13] M. Drescher and F. Krausz, J. Phys. B: At., Mol. Opt. Phys. **38**, S727 (2005).

[14] A. Maquet and R. Taïeb, J. Mod. Opt. **54**, 1847 (2007).

[15] S. Düsterer, L. Rading, P. Johnsson, A. Rouzée, A. Hundertmark, M. J. J. Vrakking, P. Radcliffe, M. Meyer, A. K. Kazansky, and N. M. Kabachnik, J. Phys. B: At., Mol. Opt. Phys. **46**, 164026 (2013).

[16] J. Itatani, F. Quéré, G. L. Yudin, M. Y. Ivanov, F. Krausz, and P. B. Corkum, Phys. Rev. Lett. **88**, 173903 (2002).

[17] U. Frühling, M. Wieland, M. Gensch, T. Gebert, B. Schutte, M. Krikunova, R. Kalms, F. Budzyn, O. Grimm, J. Rossbach, E. Plonjes, and M. Drescher, Nat. Photon. **3**, 523 (2009).

[18] F. Krausz and M. Ivanov, Rev. Mod. Phys. **81**, 163 (2009).

[19] R. Pazourek, S. Nagele, and J. Burgdörfer, Rev. Mod. Phys. **87**, 765 (2015).

[20] R. Taïeb, V. Véniard, A. Maquet, N. L. Manakov, and S. I. Marmo, Phys. Rev. A **62**, 013402 (2000).

[21] A. K. Kazansky, A. V. Grigorieva, and N. M. Kabachnik, Phys. Rev. A **85**, 053409 (2012).

[22] A. K. Kazansky, A. V. Bozhevolnov, I. P. Sazhina, and N. M. Kabachnik, J. Phys. B: At., Mol. Opt. Phys. **47**, 065602 (2014).

[23] T. Mazza, E. Gryzlova, A. Grum-Grzhimailo, A. Kazansky, N. Kabachnik, and M. Meyer, J. Electron Spectrosc. Relat. Phenom. **204, Part B**, 313 (2015).

[24] M. Richter, M. Kunitski, M. Schöffler, T. Jahnke, L. P. H. Schmidt, M. Li, Y. Liu, and R. Dörner, Phys. Rev. Lett. **114**, 143001 (2015).

[25] L. H. Haber, B. Doughty, and S. R. Leone, J. Phys. Chem. A **113**, 13152 (2009).

[26] S. Mondal, H. Fukuzawa, K. Motomura, T. Tachibana, K. Nagaya, T. Sakai, K. Matsunami, S. Yase, M. Yao, S. Wada, H. Hayashita, N. Saito, C. Callegari, K. C. Prince, C. Miron, M. Nagasono, T. Togashi, M. Yabashi, K. L. Ishikawa, A. K. Kazansky, N. M. Kabachnik, and K. Ueda, Phys. Rev. A **89**, 013415 (2014).

[27] L. V. Keldysh, ZhETF **47**, 1945 (1965) [JETP **20**, 1307 (1965)].

[28] F. H. M. Faisal, J. Phys. B: At. Mol. Phys. **6**, L89 (1973).

[29] H. R. Reiss, Phys. Rev. A **22**, 1786 (1980).

[30] M. Meyer, D. Cubaynes, P. O'Keeffe, H. Luna, P. Yeates, E. T. Kennedy, J. T. Costello, P. Orr, R. Taïeb, A. Maquet, S. Düsterer, P. Radcliffe, H. Redlin, A. Azima, E. Plönjes, and J. Feldhaus, Phys. Rev. A **74**, 011401(R) (2006).

[31] A. K. Kazansky and N. M. Kabachnik, J. Phys. B: At., Mol. Opt. Phys. **43**, 035601 (2010).

[32] A. K. Kazansky, I. P. Sazhina, and N. M. Kabachnik, Phys. Rev. A **82**, 033420 (2010).

[33] S. Bivona, G. Bonanno, R. Burlon, and C. Leone, Laser Phys. **20**, 2036 (2010).

[34] A. A. Gramajo, R. Della Picca, C. R. Garibotti, and D. G. Arbó, Phys. Rev. A **94**, 053404 (2016).

[35] L. H. Haber, B. Doughty, and S. R. Leone, Mol. Phys. **108**, 1241 (2010).

[36] P. A. Macri, J. E. Miraglia, M. S. Grabielle, F. D. Colavecchia, C. R. Garibotti, and G. Gasaneo, Phys. Rev. A **57**, 2223 (1998).

[37] D. G. Arbó, J. E. Miraglia, M. S. Gravielle, K. Schiessl, E. Persson, and J. Burgdörfer, Phys. Rev. A **77**, 013401 (2008).

[38] D. Wolkow, Z. Phys. **94**, 250 (1935).

[39] S. Nagele, R. Pazourek, J. Feist, K. Doblhoff-Dier, C. Lemell, K. Tökési, and J. Burgdörfer, J. Phys. B: At., Mol. Opt. Phys. **44**, 081001 (2011).

[40] R. Della Picca, J. Fiol, and P. D. Fainstein, J. Phys. B: At., Mol. Opt. Phys. **46**, 175603 (2013).

[41] C. C. Chirilă and R. M. Potvliege, Phys. Rev. A **71**, 021402(R) (2005).

[42] P. B. Corkum, N. H. Burnett, and M. Y. Ivanov, Opt. Lett. **19**, 1870 (1994).

[43] M. Ivanov, P. B. Corkum, T. Zuo, and A. Bandrauk, Phys. Rev. Lett. **74**, 2933 (1995).

[44] M. Lewenstein, K. C. Kulander, K. J. Schafer, and P. H. Bucksbaum, Phys. Rev. A **51**, 1495 (1995).

[45] D. G. Arbó, K. L. Ishikawa, K. Schiessl, E. Persson, and J. Burgdörfer, Phys. Rev. A **81**, 021403 (2010).

[46] D. G. Arbó, K. L. Ishikawa, K. Schiessl, E. Persson, and J. Burgdörfer, Phys. Rev. A **82**, 043426 (2010).

[47] X.-M. Tong and S. I. Chu, Chem. Phys. **217**, 119 (1997).

[48] X.-M. Tong and S.-I. Chu, Phys. Rev. A **61**, 031401(R) (2000).

[49] X. M. Tong and C. D. Lin, J. Phys. B: At., Mol. Opt. Phys. **38**, 2593 (2005).

[50] Here the $2\pi$ equivalence $a \equiv b$ means that $(a - b)/2\pi$ is an integer and $0 \leqslant \phi < 2\pi$.